Electronic Supplementary Material (ESI) for Journal of Materials Chemistry C.

Supporting Information

Antiferromagnetic Quaternary Chalco-Halide $Ba_3(FeS_4)I$ with Long Fe···Fe Distances

Yi Xiao,[a, b] Xian Zhang,*[, b] Ruiqi Wang,[a] Simin An,[c] Fuqiang Huang*[,a,d]

[a]Beijing National Laboratory for Molecular Sciences and State Key Laboratory of Rare Earth Materials Chemistry and Applications, College of Chemistry and Molecular Engineering, Peking University, 202 Chengfu Road, Beijing 100871, P.R. China.

E-mail: huangfq@pku.edu.cn

[b]Qian Xuesen Laboratory of Space Technology, China Academy of Space Technology, Beijing 100094, P. R. China.

E-mail: zhangxian@qxslab.cn

[c]Laboratory of Computational Physics, Institute of Applied Physics and Computational Mathematics, Beijing 100088, P. R. China.

[d]Department CAS Key Laboratory of Materials for Energy Conversion Shanghai Institute of Ceramics, Chinese Academy of Sciences, 1295 Dingxi Road, Shanghai 200050, P.R. China.

EXPERIMENTAL SECTION

Reagent. All the starting materials are obtained from Sinopharm Chemical Reagent Beijing Co., Ltd: (i) barium pieces, AR, 99.5%, (ii) iron powder, AR, 99.9%; (vi) sulfur powder, sublimed, 99.9%; (iii) iodine pieces, AR, 99.9%. All the reagents are kept in an Ar-protected glove box. No further purifications were performed before use.

Synthesis of $Ba_3(FeS_4)I$ single crystals. Starting materials of Ba pieces (0.412 g, 3 mmol), Fe powder (0.056 g, 1 mmol), S powder (0.128 g, 4 mmol), iodine pieces (0.127 g, 1 mmol) and KI (5 g, 30 mmol) were weighted and loaded into a carbon coated silica tube. The tube was flame-sealed under vacuum (10^{-3} mbar) and heated slowly to 1173 K with a programmable furnace. The reaction was kept at this temperature for 4 days followed by cooling to 773 K at a rate of 2 K/h. Finally, the silica tube was quenched in air. The direct combination reaction at the presence of excess KI flux gave solidified melts. The melts were washed and sonicated by distilled water and dried with acetone. Then the black $Ba_3(FeS_4)I$ crystals were obtained.

Single Crystal X-ray Crystallography. Single crystals suitable for X-ray diffraction were chosen from the as-prepared samples. Data collection was performed on an *Agilent Super Nova Diffractometer* equipped with mirror-monochromated Mo-K_α radiation. The structures of the two compounds were solved by direct methods and refined by full-matrix least-squares on F^2 using the SHELXTL program package. Multi-scan absorption corrections were performed. The crystal data and refinement details are summarized in Table 1.

Table 1. Crystallographic data and details of the structure refinement for $Ba_3(FeS_4)I$

formula	**$Ba_3(FeS_4)I$**
F_w (g·mol^{-1})	722.98
crystal system	Orthorhombic
space group	*Cmcm*
a (Å)	6.8817(4)
b (Å)	15.894(1)
c (Å)	9.6864(8)
α (°)	90
β (°)	90
γ (°)	90
V (Å^3)	1059.5(1)
ρ_c (g·cm^{-3})	4.533
μ (mm^{-1})	15.970
F(000)	1244
R_{int}	0.0164
R [$I > 2\sigma(I)$]	0.0224
wR_2 (all data)	0.0501
GOF	1.168

Powder X-ray Diffraction (PXRD). The synthesized crystal samples were ground and used to verify the phase purity on a Rigaku X-ray diffractometer (Cu K_α). Simulated patterns were generated using the CrystalMaker program and the CIF of the refined structure.

UV-vis Light Spectroscopy. Optical diffuse-reflectance measurements were carried out using a UV-4100 spectrophotometer operating from 2000 nm to 300 nm at room temperature. The $BaSO_4$ powder was used as a 100% reflectance standard. The powder samples were spread on a compacted base of $BaSO_4$ powder. The generated reflectance-versus-wavelength data were used to measure the band gap of the material. The reflectance data was converted to absorbance data using the Kubelka-Munk equation.

Magnetic Property Measurements. The magnetic properties of the as-prepared compounds were studied using a superconducting quantum interference device magnetometer (Quantum design, MPMS). The DC susceptibility measurements, both under zero-field-cooling (ZFC) and field-cooling (FC) conditions, were performed in a 1000 Oe magnetic field for temperatures ranging from 2 to 300 K.

Electronic Structure Calculations. The first-principles computations based on the density-functional theory (DFT) were performed using the Vienna Ab-initio Simulation Package (VASP). The Perdew-Burke-Ernzerhof (PBE) version of the generalized gradient approximation (GGA) was used to describe the exchange correlation function and the projector augmented wave (PAW) method was used in the present work. Here, the cutoff energy of plane wave was chosen at 350 eV. For the structure optimizations, 6×6×6 Monkhorst-Pack grids were used for the primitive cell (AFM6 used a double size cell) and 4×4×4 k-points for the conventional cell, respectively. The relaxation of geometry optimization was performed until the total energy changes within 10^{-6} eV/atom and the Hellmann-Feynman force on all atomic sites was less than 0.01 eV/Å.

Table S1. Relative energies of $Ba_3(FeS_4)I$ in different magnetic states with respect to the nonmagnetic state (unit in eV/Fe).

Magnetic orders	E_0 **(eV/Fe)**
AFM1 (2 up and 2 down)	**-2.289**
AFM2 (2 up and 2 down)	-2.283
AFM3 (2 up and 2 down)	-2.271
AFM4 (2 up and 2 down)	-2.242
AFM5 (3 up and 1 down)	-2.256
AFM6 (3 up and 1 down)	-2.256
Ferromagnetic (4 spin up)FM	-2.229

Table S2 Atomic coordinates, equivalent isotropic displacement parameters (Å^2) and bond valence sum (BVS) of $Ba_3(FeS_4)I$

Label	***x/a***	***y/b***	***z/c***	***SOF***	**U_{eq}***	**BVS**
Ba1	0	0.8258(1)	0.9788(1)	1	0.0115(1)	+2.0
Ba2	0.5	0.9480(1)	0.25	1	0.0102(1)	+2.6
Fe	0	0.0018(1)	0.25	1	0.0084(3)	+3.0
S1	0	0.6136(1)	0.0523(1)	1	0.0171(3)	-2.2
S2	0.2439(2)	0.7268(1)	0.75	1	0.0109(3)	-1.8
I	0	0.0017(1)	0.75	1	0.0148(2)	-1.6

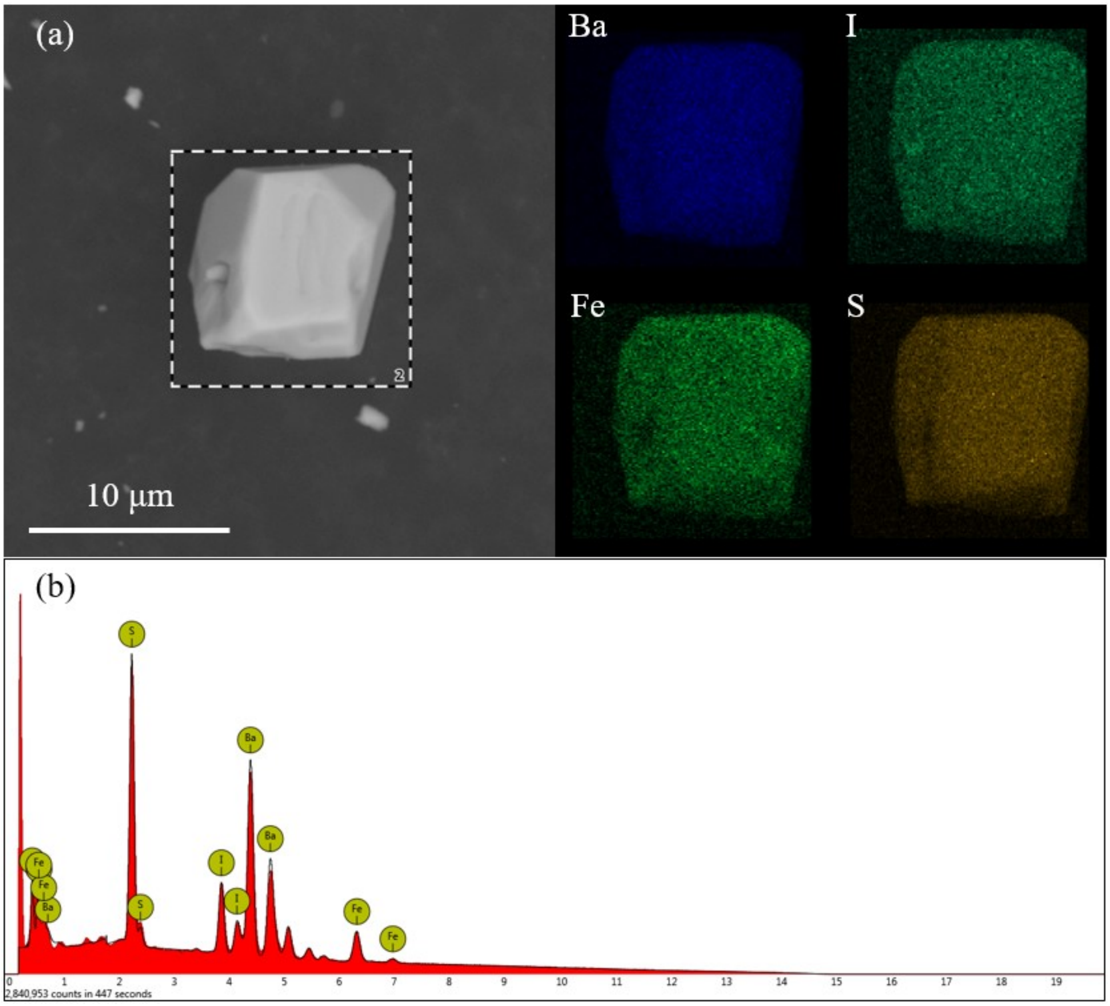

Figure S1. SEM image and EDX spectrum of a $Ba_3(FeS_4)I$ single crystal.

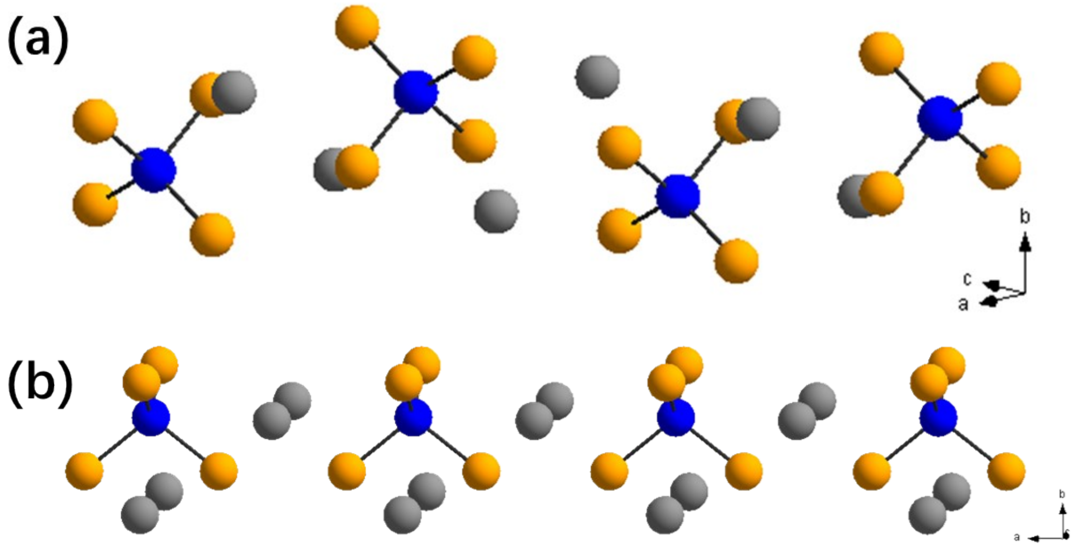

Figure S2. The arrangement of FeS_4 tetrahedral along the [101] direction (a) and the a axis (b) in $Ba_3(FeS_4)I$. Fe, S, and Ba, are represented by blue, orange, and grey spheres, respectively.

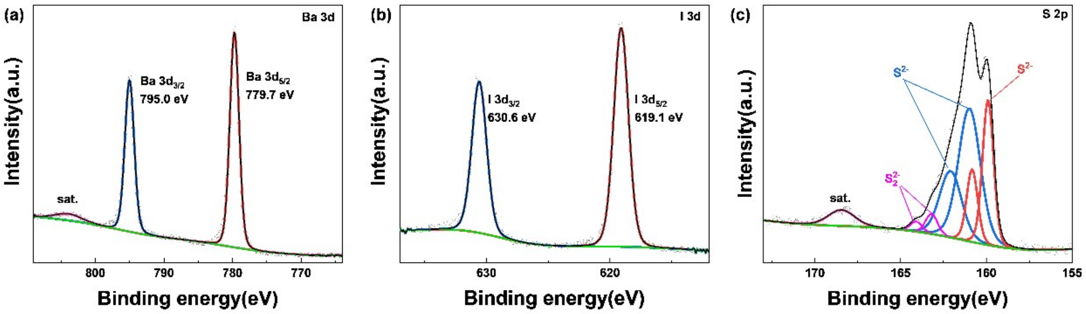

Figure S3. XPS spectra of Ba (a), I (b), and S (c) of $Ba_3(FeS_4)I$.

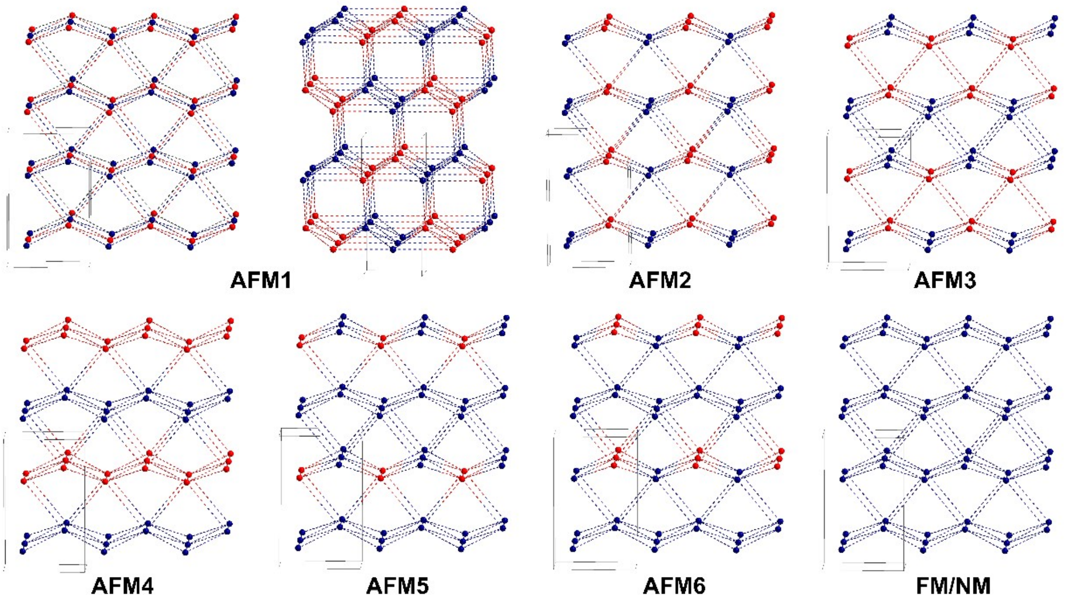

Figure S4. Seven possible magnetic orders of $Ba_3(FeS_4)I$. The red and blue balls denote the Fe atoms with spin up and spin down, respectively. For clarity, the Ba and Br atoms have not been shown.

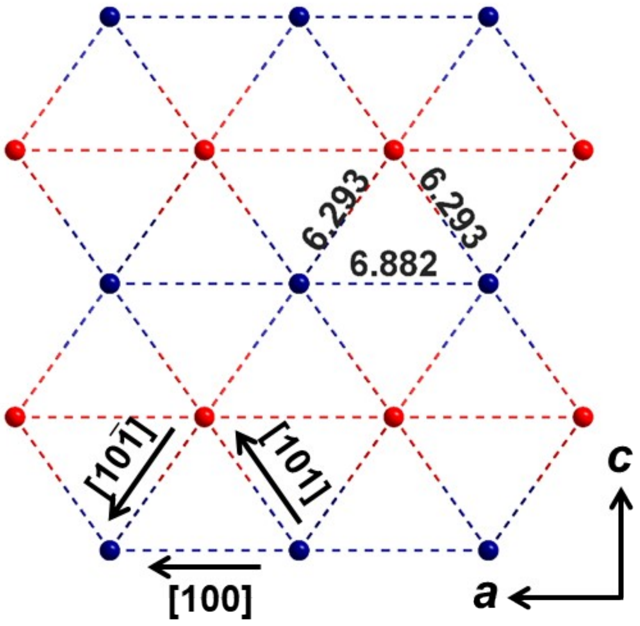

Figure S5. Spin ordering of Fe atoms between two adjacent $[IBa_3]^{5+}$ layers in AFM2 order.

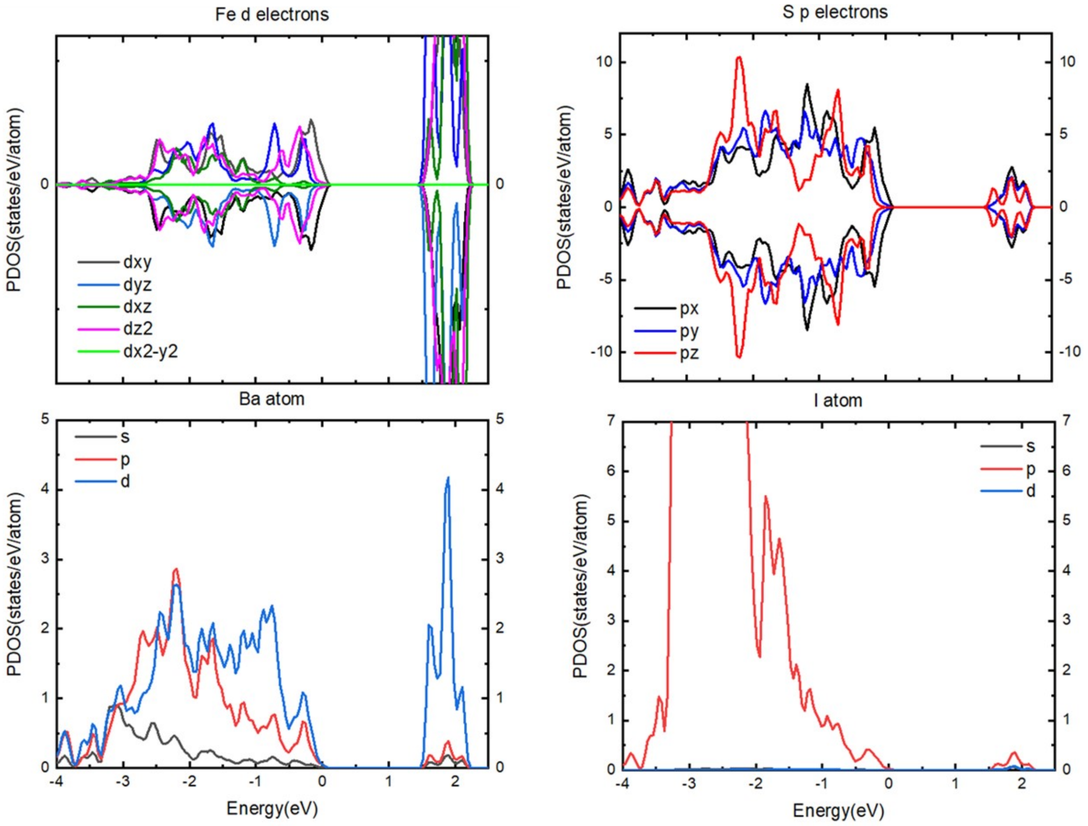

Figure S6. Partial density of states of $Ba_3(FeS_4)I$ with AFM1 order.

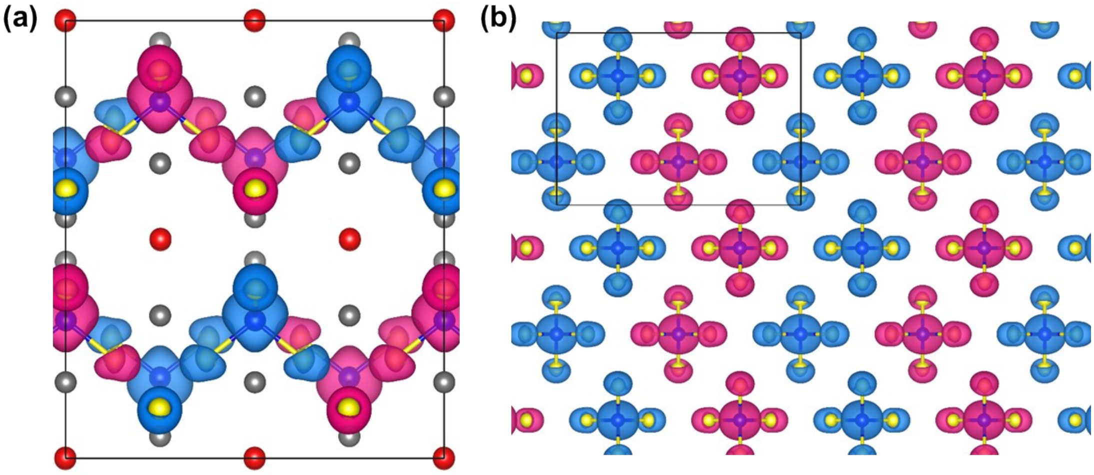

Figure S7. Spin density of $Ba_3(FeS_4)I$ in the AFM1 order. The Ba and Br atoms are omitted for clarity.